Computer Aided Geometric Design 105 (2023) 102222

Contents lists available at ScienceDirect

Computer Aided Geometric Design

journal homepage: www.elsevier.com/locate/cagd

Blending Bézier patch for multi-sided surface modeling ☆

Kaikai Qin, Yajuan Li, Chongyang Deng *

School of Science, Hangzhou Dianzi University, China

ARTICLE INFO

Article history:
Received 4 May 2022
Received in revised form 16 May 2023
Accepted 10 June 2023
Available online 16 June 2023

Keywords:
Multi-sided Bézier patch
Gregory corner blending
G^2 continuity
Free-form surfaces
Hole filling

ABSTRACT

This study proposes a new n-sided ($n \geq 4$) control point-based surface patch, the blending Bézier patch (BB patch), by constructing corner Bézier surfaces and using Gregory corner blending. A BB patch is defined on a regular polygonal domain with an n-sided control net generalized from quadrilateral Bézier grids, and it reduces to the same degree as a Bézier patch when $n = 4$. There are two main steps for constructing a BB patch: defining a corner Bézier patch for each corner and blending all corner Bézier patches using rational blending functions. Because the boundary behaviors of the BB patch are similar to those of the Bézier patch, a BB patch can be easily joined to the surrounding Bézier and other BB patches. As an application, we used BB patches to fill the holes with G^2 continuity.

1. Introduction

Tensor-product Bézier patches are typically used for free-form surface modeling in the field of computer aided geometric design (CAGD). In general, a complex object cannot be represented by just a single patch; therefore, a set of smoothly connected patches is required. Patchwork (multi-patch surface) is usually assembled using regular (quadrilateral) patches. However, multi-sided Bézier patches are often required to fill n-sided holes (Goldman, 2004) when irregular (non-four-sided) regions occur. Thus, constructing multi-sided free-form surfaces is an important topic in the field of CAGD.

Multifarious methods exist for generating multi-sided surfaces that have different features and satisfy various requirements (see a detailed review of Peters (2019)). We specifically focus on "genuine" n-sided patches that usually directly map planar n-sided domains to n-sided surfaces in space. This includes techniques such as multi-sided transfinite interpolation and multi-sided control point-based surfaces.

In 2016, Várady et al. combined the transfinite construction (side interpolant (Salvi et al., 2014)) and control point-based scheme to create their multi-sided Bézier patch — the generalized Bézier (GB) patch (Várady et al., 2016). The GB patch has good properties and there has been a series of excellent researches based on GB patch, such as (Várady et al., 2017; Salvi and Várady, 2018).

In this study, we combine the Gregory corner blending (Charrot and Gregory, 1984; Gregory and Hahn, 1989) and the tensor-product Bézier scheme to define a new n-sided ($n \geq 4$) control point-based surface, that is, the Blending Bézier patch (BB patch). The BB patch has a simple and intuitive control structure. The patch evaluation does not include any weight deficiency or an additional correction term. The BB patch possesses tensor-product Bézier patch boundaries; thus, it can be smoothly connected to the adjacent ordinary quadrilateral Bézier or other BB patches. In addition, the BB scheme produced an ordinary quadrilateral Bézier patch when $n = 4$.

☆ Editor: Tamas Varady.

* Corresponding author.
E-mail address: dcy@hdu.edu.cn (C. Deng).

https://doi.org/10.1016/j.cagd.2023.102222
0167-8396/

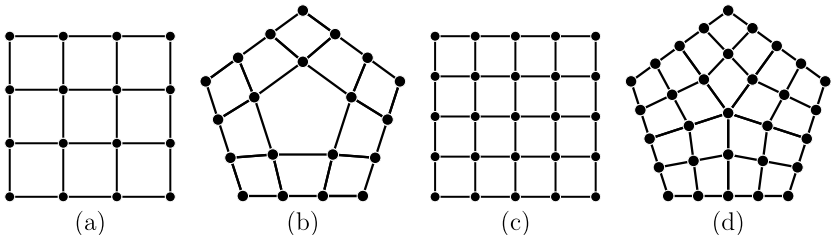

Fig. 1. Four-sided and five-sided grids: (a) 4-sided, degree 3; (b) 5-sided, degree 3; (c) 4-sided, degree 4; (d) 5-sided, degree 4.

The remainder of this paper is organized as follows. In Section 2, we provide a brief overview of related works. Details of constructing the BB patch, including the control nets, local parameters, blending functions, and the boundary behavior of the BB patch are presented in Section 3. In Section 4, we present some examples to illustrate the features of BB patches. We discuss the limitations of BB patches and further work in Section 5 before concluding the paper in Section 6.

2. Related works

A rich body of literature involves the construction of multi-sided patches. In this section, we provide a brief overview of related works.

Subdivision schemes are effective methods for constructing surfaces from arbitrary topology meshes via infinite recursive refinement. The traditional Catmull–Clark subdivision generates C^2 limit surfaces in regular regions, but only holds C^1 continuity over extraordinary vertices (Catmull and Clark, 1978). Karčiauskas and Peters (2007) proposed a guided subdivision scheme that can generate global curvature continuous subdivision surfaces. However, achieving accurate interpolation of boundaries, including cross-derivatives, using the limit surface poses a challenging problem.

Another way of constructing smooth multi-sided surfaces involves using macro-patches. An n-sided macro-patch consists of n smoothly connected quadrilateral patches; all of these patches share one corner vertex, and every two adjacent patches share one boundary curve. Gregory and Zhou (1994) first constructed a C^1 macro-patch of degree bi-3, followed by Peters' (1999) C^1 multi-sided surfaces of degrees bi-2 and bi-3. Loop and Schaefer (2008) generated G^2 continuous macro-patches of degree bi-7. Recently, Karčiauskas and Peters (2016, 2020) and Peters constructed their bi-6 G^2 macro-patches.

The multi-sided transfinite construction generates surfaces by interpolating the given boundary data, while the interior is automatically assembled. Research on multi-sided transfinite surfaces started with Charrot and Gregory (1984), who generated their C^1 pentagonal patches using corner interpolants, followed by a C^2 polygonal patch (Gregory and Hahn, 1989). Then, Kato (1991) defined the n-sided patches with holes via side interpolants; and Várady (1991) defined the overlapping patches. In 2011, Várady et al. (2011) studied transfinite surfaces over irregular n-sided domains. Later, Salvi et al. proposed ribbon-based transfinite surfaces (Salvi et al., 2014) and extended the G^2 Gregory patches (Salvi and Várady, 2014).

Multi-sided control point-based schemes produce n-sided surfaces with multiple local controls. Sabin (1983) first constructed three- and five-sided patches with quadratic boundaries. Hosaka and Kimura (1984) defined similar cubic patches with three, five and six sides. Zheng and Ball (1997) extended these quadratic and cubic patches to arbitrary degrees on three, five, and six sides. Loop and DeRose (1989) extended the tensor-product Bézier and triangular Bézier patches to construct an S-patch using multivariate Bernstein polynomials. Warren (1992) constructed four-, five-, and six-sided rational Bézier surfaces from rational triangular Bézier patches with base points. All these methods are bound by the number of sides, except for the S-patch.

Várady et al. proposed a multi-sided control-point-based scheme, the generalized Bézier (GB) patch (Várady et al., 2016), which is defined as a linear combination of a series of half-Bézier ribbons. Each half-Bézier ribbon consists of half-Bézier control points multiplied by the corresponding weighted Bernstein functions. The GB patches are compatible with adjacent ordinary quadrilateral Bézier patches (G^1 or G^2). However, weight deficiency must to be considered to ensure that the sum of all the blending functions is equal to one.

3. Blending Bézier patch

An n-sided ($n \geq 4$), degree d BB patch is defined over a regular n-sided polygonal domain Ω with vertices $\{V_i\}_{i=0}^{n-1}$.[1] Each side of the polygon $\Gamma_i = \{(1-\lambda)V_i + \lambda V_{i+1} \mid 0 \leq \lambda \leq 1\}$ is mapped to a degree d Bézier curve. The control nets of BB patches are generalized from the control nets of Bézier surfaces, same as the improved GB patches (Várady et al., 2017), called rectangular spider webs in Goldman (2004). The control net of a degree d, n-sided BB patch has $nl(l+1)+1$ control points for even degrees ($d = 2l$) and has $n(l+1)^2$ control points for odd degrees ($d = 2l+1$) (see Fig. 1). We stress that

[1] We use circular index.

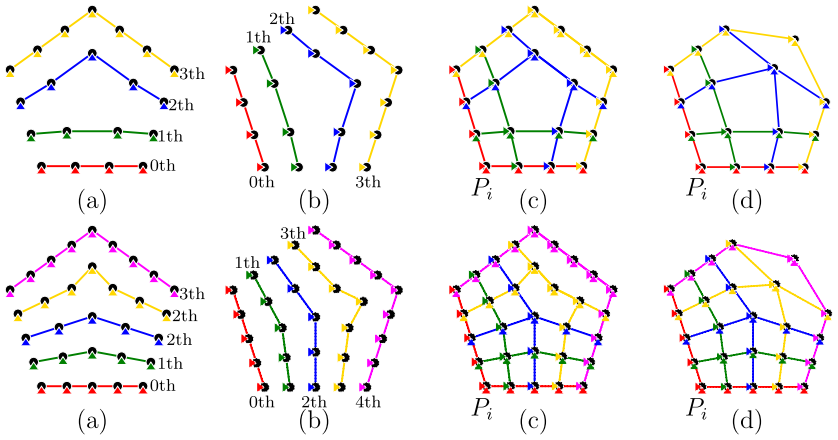

Fig. 2. Constructing corner control nets: (a)-(c) The division around the ith corner point of a 5-sided, degree 3 grid; (d) the i-th corner control net of a 5-sided, degree 3 grid; (e)-(g) the division around the ith corner point of a 5-sided, degree 4 grid; (h) the i-th corner control net of a 5-sided, degree 4 grid.

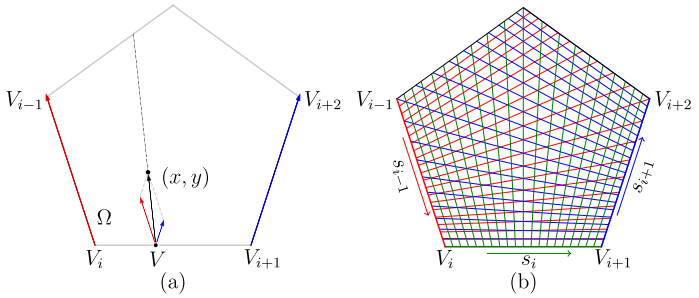

Fig. 3. Constrained parameterization. (a) Construction of the constrained parameterization; (b) Isolines of s_{i-1} (in red), s_i (in green) and s_{i+1} (in blue). (For interpretation of the colors in the figure(s), the reader is referred to the web version of this article.)

the input multi-sided Bézier control net assumes twist compatibility, indicating that the scheme only allows the use of twist-compatible data.

In the following, we first introduce the corner Bézier patch in Section 3.1, which includes three subsections for corner control net (Section 3.1.1), local parameters (Section 3.1.2), and the equation of the corner Bézier patch (Section 3.1.3). The blending functions are presented in Section 3.2. Subsequently, we formulate the surface equation of the BB patch in Section 3.3. Furthermore, the boundary behavior of the BB patch is investigated in the Section 3.4.

3.1. Corner Bézier patch

For each corner point P_i $(i = 0, ..., n-1)$ of an n-sided degree d ($d = 2l$ or $2l+1$) grid, we define a degree d corner Bézier patch as the corner interpolant.

3.1.1. Corner control net

To construct the control net of degree d corner Bézier patch, we selected $(d+1)^2$ control points from the n-sided, degree d control net for each corner point P_i. It is well known that a four-sided degree d Bézier control net has $(d+1)^2$ control points that belong to $d+1$ rows or $d+1$ columns. Thus we divided the control points of an n-sided degree d control net into $d+1$ rows and $d+1$ columns around the ith corner point P_i. Fig. 2 shows the division: control points that belong to the same row are marked by the same colored upward-facing triangle (Figs. 2 (a) and (e)), and control points that belong to the same column are marked by the same colored right-facing triangle (Figs. 2 (b) and (f)). Control points that belong to the same row and same column are marked by the same colored upward-facing and right-facing triangles (Figs. 2 (c) and (g)). Then, for each point of the grid, we define an index $(j,k)^i$ called the ith corner index: j implies that it belongs to the $(j+1)$th row, k indicates that it belongs to the $(k+1)$th column, and i indicates that the division is around the ith corner point P_i (see Figs. 2 (a)–(c), (e)–(g)).

We used the set $\mathcal{P}^i_{j,k}$ to represent all the points whose ith corner indexes are $(j,k)^i$, and $|\mathcal{P}^i_{j,k}|$ is the number of elements of the set $\mathcal{P}^i_{j,k}$. Then, the ith corner control net, denoted by $\{\mathbf{b}^i_{j,k}\}$ where $j,k = 0, ..., d$, is defined as follows:

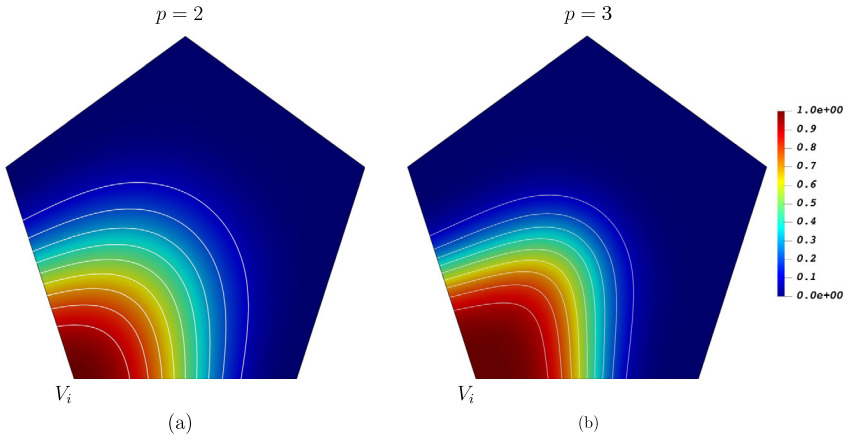

Fig. 4. Corner blending functions. (a) α_i with $p = 2$; (b) α_i with $p = 3$.

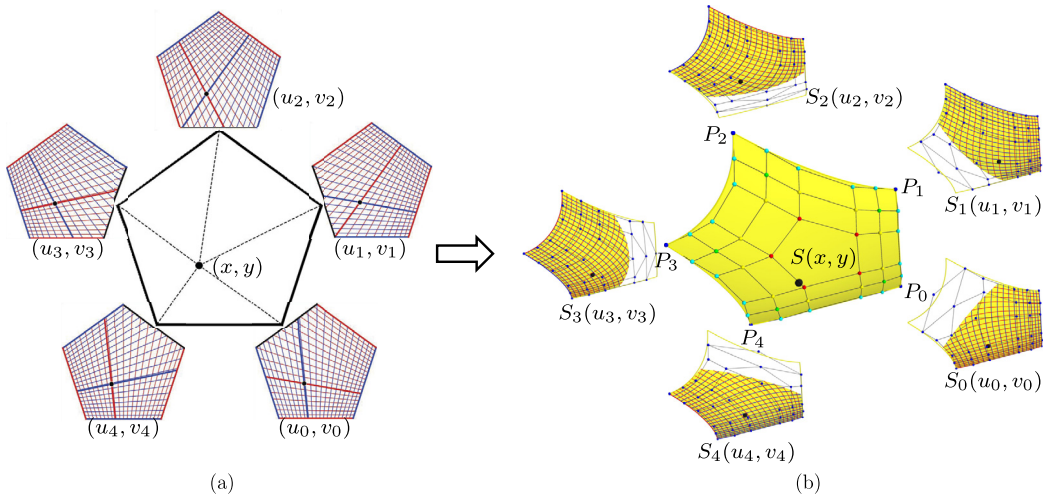

Fig. 5. A 5-sided BB patch evaluation: (a) Regular pentagonal domain and local parameters; (b) corner Bézier patches and the final BB patch.

$$\mathbf{b}^i_{j,k} = \frac{\sum_{\mathbf{p}\in\mathcal{P}^i_{j,k}} \mathbf{p}}{|\mathcal{P}^i_{j,k}|}. \tag{1}$$

This implies that the control points, marked by the same colored upward-facing and right-facing triangles in Figs. 2 (c) and (g), were averaged into one point, as shown in Figs. 2 (d) and (h).

Clearly, the ith corner control net preserves the positions of several points, including the first $l+1$ rows and columns around the ith corner. Thus we have,

$$\mathbf{b}^i_{j,k} = \mathbf{b}^{i+1}_{d-k,j}, \quad 0 \le j \le l, 0 \le k \le d. \tag{2}$$

3.1.2. Local parameters — Salvi and Várady's parameterization

For each corner vertex of the regular polygonal domain (also each corner control net), we required two local parameters u_i and v_i. Here, we used the constrained sweep parameterization proposed by Salvi and Várady (2014), which can ensure G^2 interpolation, to determine the local parameters.

The constrained sweep parameterization was constructed using the Hermite polynomials. Let (x, y) be an arbitrary point in the polygonal domain, and let $V = (1 - s_i)V_i + s_i V_{i+1}$ $(s_i \in [0, 1])$ be the associated point on the ith side and $\overrightarrow{V_i V_{i-1}}$ and $\overrightarrow{V_{i+1} V_{i+2}}$ edge vectors, as shown in Fig. 3 (a). The constrained sweep parameter s_i is subject to an equation that is formulated as follows.

$$(x, y) = V + h_i[H(s_i)\overrightarrow{V_i V_{i-1}} + H(1 - s_i)\overrightarrow{V_{i+1} V_{i+2}}], \tag{3}$$

where $H(s_i) = 2s_i^3 - 3s_i^2 + 1$ is the third-degree Hermite polynomial and s_i and h_i are unknown. As the parameter domain is a regular polygon, h_i can be computed using the following formula:

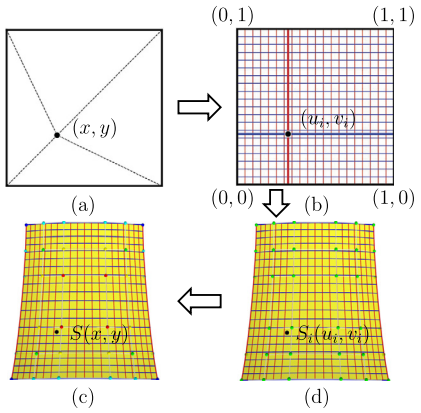

Fig. 6. (a) A square domain; (b) local parameters; (c) corner Bézier patch; (d) the 4-sided BB patch.

$$h_i = \frac{d_i}{||\overrightarrow{V_i V_{i+1}}|| \cdot \sin\frac{2\pi}{n}}, \tag{4}$$

where d_i is the perpendicular distance from point (x, y) to side Γ_i, and $||\overrightarrow{V_i V_{i+1}}||$ is length of the ith side. Thus, we can obtain the value of s_i by solving the Equation (3), and Fig. 3 (b) shows the constant lines of the parameterization. The parameter s_i increases linearly on side Γ_i and is 0 on side Γ_{i-1} and 1 on side Γ_{i+1}.

Then, the two local parameters u_i and v_i are defined as

$$u_i = s_i,\ v_i = 1 - s_{i-1}. \tag{5}$$

According to this special construction of the parameterization, the local parameters satisfy the following constraints:

$$\left.\frac{\partial u_{i+1}}{\partial u_i}\right|_{\Gamma_i} = 0,\ \left.\frac{\partial v_{i+1}}{\partial u_i}\right|_{\Gamma_i} = -1,\ \left.\frac{\partial u_{i+1}}{\partial v_i}\right|_{\Gamma_i} = 1,\ \left.\frac{\partial v_{i+1}}{\partial v_i}\right|_{\Gamma_i} = 0. \tag{6}$$

3.1.3. Equation of corner Bézier patch

Using the corner control net and two local parameters u_i and v_i, the ith corner Bézier patch S_i is defined as follows:

$$S_i(u_i, v_i) = \sum_{j=0}^{d}\sum_{k=0}^{d} B_k^d(u_i) B_j^d(v_i) \mathbf{b}_{j,k}^i, \tag{7}$$

where

$$B_k^d(u_i) = \binom{d}{k} \cdot (1-u_i)^{d-k} u_i^k,\ B_j^d(v_i) = \binom{d}{j} \cdot (1-v_i)^{d-j} v_i^j,$$

are the Bernstein basis functions.

3.2. Blending functions

We used the traditional Gregory corner blending functions (Charrot and Gregory, 1984; Gregory and Hahn, 1989) to combine these n corner Bézier patches. The corner blending functions take values between 0 and 1 on the adjacent sides, and vanish on the nonadjacent sides. The function α_i (for $i = 0, \ldots, n-1$) is defined as follows:

$$\alpha_i = \frac{\lambda_i^p}{\sum_{q=0}^{n-1} \lambda_q^p}, \tag{8}$$

where $\lambda_i = \prod_{j \neq i-1, i} d_j$, $p = 2$ for G^1 interpolation and $p = 3$ for G^2 interpolation. Fig. 4 shows the distribution of the corner blending function α_i over the regular pentagonal domain.

Furthermore, on side Γ_i, the blending functions satisfy the following two constraints:

$$\begin{aligned} &(\alpha_i + \alpha_{i+1})\big|_{\Gamma_i} = 1, \\ &\alpha_j\big|_{\Gamma_i} = 0,\ j \neq i, i+1, \end{aligned} \tag{9}$$

and

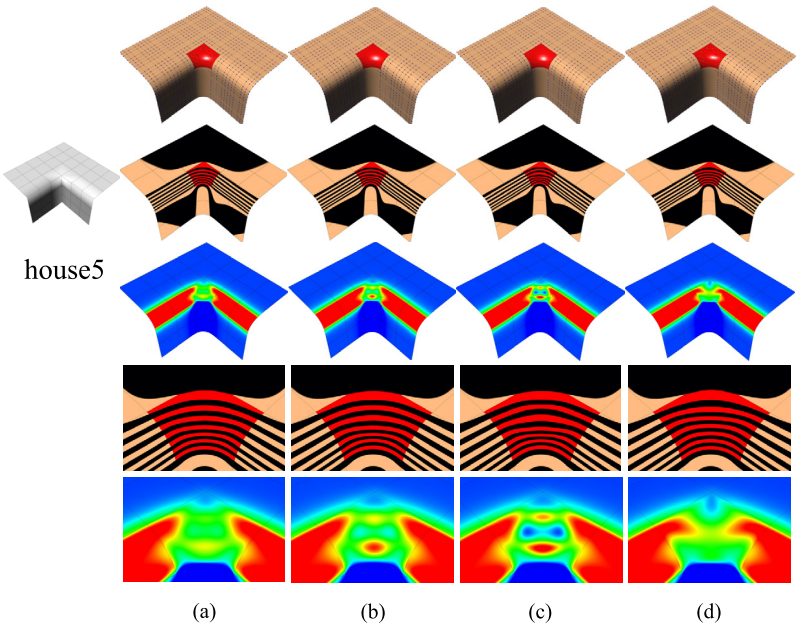

Fig. 7. house5. Fill a 5-sided hole with G^2 continuity in different methods. (a) The BB patch; (b) Gregory patch (Gregory and Hahn, 1989); (c) extended G^2 Gregory patch (Salvi and Várady, 2014); (d) the GB patch (Várady et al., 2017). From top to bottom: shaded multi-sided patch with surrounding regular patches, reflection lines, mean curvature, close-up of reflection lines and close-up of mean curvature.

$$\begin{aligned} &\frac{\partial^m \alpha_j}{\partial w^m}\bigg|_{\Gamma_i} = 0, \ j \neq i, i+1, \\ &\left(\frac{\partial^m \alpha_i}{\partial w^m} + \frac{\partial^m \alpha_{i+1}}{\partial w^m}\right)\bigg|_{\Gamma_i} = 0, \end{aligned} \tag{10}$$

where $1 \leq m \leq p-1$ and w denotes an arbitrary direction in the polygonal domain. The blending functions can ensure that only the corner Bézier patches S_i and S_{i+1} influence on side Γ_i.

3.3. Patch equation

The BB patch is defined based on the blending functions and corner Bézier surfaces, as follows:

$$S^{d,n,p}(x,y) = \sum_{i=0}^{n-1} \alpha_i S_i(u_i, v_i) = \sum_{i=0}^{n-1} \frac{\lambda_i^{\ p}}{\sum_{q=0}^{n-1} \lambda_q^{\ p}} \sum_{j=0}^{d} \sum_{k=0}^{d} B_k^d(u_i) B_j^d(v_i) \mathbf{b}_{j,k}^i. \tag{11}$$

Fig. 5 shows the process of a five-sided BB patch evaluation. Based on $\sum_{j=0}^{d} \sum_{k=0}^{d} B_k^d(u_i) B_j^d(v_i) = 1$ and $\sum_{i=0}^{n-1} \alpha_i = 1$, the sum of all weights $\{\alpha_i B_k^d(u_i) B_j^d(v_i)\}_{i,j,k=0}^{n-1,d,d}$ is equal to one.

Note that, in the case of $n = 4$, the BB patch is reduced to an ordinary Bézier patch. This is because the two local parameters reproduce the normal rectangular domain, and the corner grids are reduced to the original four-sided grid. Thus, each corner patch is exactly the original Bézier patch (see Fig. 6).

3.4. Boundary behavior

In this section, we show that the BB patch possesses tensor-product Bézier patch boundaries. However, some studies have investigated the geometric continuity of Gregory-like patches (Hall and Mullineux, 1999a; Salvi and Várady, 2014). Here, we provide a straightforward explanation by computing the directional derivatives up to and including the second-order of the BB patch (with degree $d \geq 5$ and $p = 3$) with respect to u_i and v_i on the side Γ_i.[2]

[2] With degree $d \geq 3$ and $p = 2$ for G^1 continuity.

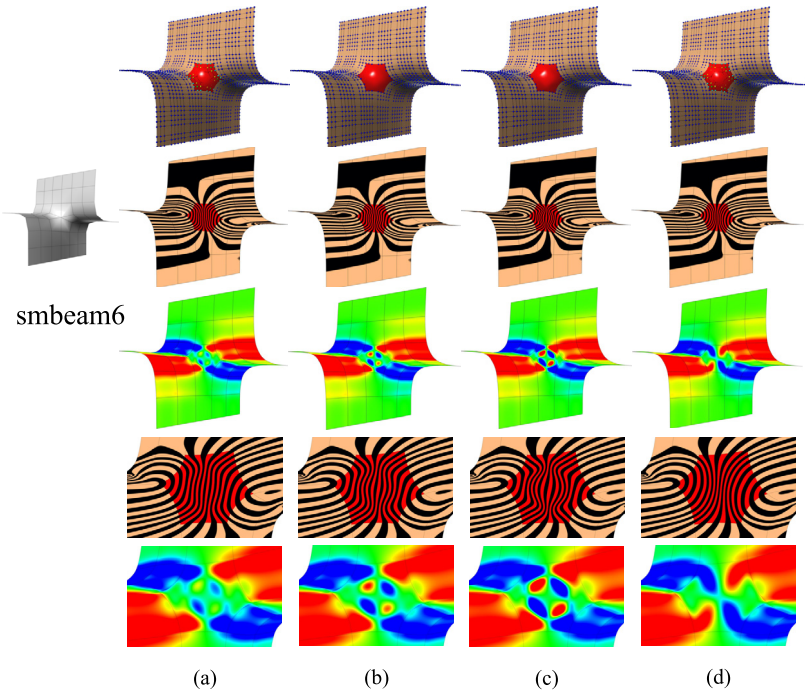

Fig. 8. smbeam6. Fill a 6-sided hole with G^2 continuity in different methods. (a) The BB patch; (b) Gregory patch (Gregory and Hahn, 1989); (c) extended G^2 Gregory patch (Salvi and Várady, 2014); (d) the GB patch (Várady et al., 2017). From top to bottom: shaded multi-sided patch with surrounding regular patches, reflection lines, mean curvature, close-up of reflection lines and close-up of mean curvature.

First, from Equation (2), we have

$$\begin{aligned} S_i\big|_{\Gamma_i} &= S_{i+1}\big|_{\Gamma_i}, \\ \frac{\partial S_i}{\partial v_i}\bigg|_{\Gamma_i} &= \frac{\partial S_{i+1}}{\partial u_{i+1}}\bigg|_{\Gamma_i}, \frac{\partial S_i}{\partial u_i}\bigg|_{\Gamma_i} = -\frac{\partial S_{i+1}}{\partial v_{i+1}}\bigg|_{\Gamma_i}, \\ \frac{\partial^2 S_i}{\partial u_i \partial v_i}\bigg|_{\Gamma_i} &= -\frac{\partial^2 S_{i+1}}{\partial v_{i+1}\partial u_{i+1}}\bigg|_{\Gamma_i}, \frac{\partial^2 S_i}{\partial v_i^2}\bigg|_{\Gamma_i} = \frac{\partial^2 S_{i+1}}{\partial u_{i+1}^2}\bigg|_{\Gamma_i}, \frac{\partial^2 S_i}{\partial u_i^2}\bigg|_{\Gamma_i} = \frac{\partial^2 S_{i+1}}{\partial v_{i+1}^2}\bigg|_{\Gamma_i}. \end{aligned} \tag{12}$$

Then, using Equations (5) and (6) and applying the chain rule, the derivatives of S_{i+1} with respect to u_i and v_i can be derived as

$$\begin{aligned} \frac{\partial S_{i+1}}{\partial v_i}\bigg|_{\Gamma_i} &= \frac{\partial S_i}{\partial v_i}\bigg|_{\Gamma_i}, \frac{\partial S_{i+1}}{\partial u_i}\bigg|_{\Gamma_i} = \frac{\partial S_i}{\partial u_i}\bigg|_{\Gamma_i}, \\ \frac{\partial^2 S_{i+1}}{\partial u_i \partial v_i}\bigg|_{\Gamma_i} &= \frac{\partial^2 S_i}{\partial u_i \partial v_i}\bigg|_{\Gamma_i} - \Big(\frac{\partial^2 v_{i+1}}{\partial u_i \partial v_i}\cdot\frac{\partial S_i}{\partial u_i}\Big)\bigg|_{\Gamma_i}, \\ \frac{\partial^2 S_{i+1}}{\partial u_i^2}\bigg|_{\Gamma_i} &= \frac{\partial^2 S_i}{\partial u_i^2}\bigg|_{\Gamma_i}, \frac{\partial^2 S_{i+1}}{\partial v_i^2}\bigg|_{\Gamma_i} = \frac{\partial^2 S_i}{\partial v_i^2}\bigg|_{\Gamma_i} + \Big(\frac{\partial^2 u_{i+1}}{\partial v_i^2}\cdot\frac{\partial S_i}{\partial v_i}\Big)\bigg|_{\Gamma_i}. \end{aligned} \tag{13}$$

Recalling Equations (9) and (12), we obtain

$$S^{d,n,3}\big|_{\Gamma_i} = S_i\big|_{\Gamma_i}. \tag{14}$$

This means that on side Γ_i, the BB patch $S^{d,n,3}$ has the same boundary curve, a degree d Bézier curve, as the corner Bézier patch S_i.

Using Equations (9), (10) and (13), the first-order derivatives of $S^{d,n,3}$ with respect to u_i and v_i can now be obtained as follows:

$$\frac{\partial S^{d,n,3}}{\partial v_i}\bigg|_{\Gamma_i} = \frac{\partial S_i}{\partial v_i}\bigg|_{\Gamma_i}, \frac{\partial S^{d,n,3}}{\partial u_i}\bigg|_{\Gamma_i} = \frac{\partial S_i}{\partial u_i}\bigg|_{\Gamma_i}. \tag{15}$$

Evidently, the BB patch $S^{d,n,3}$ interpolates the cross-derivative of the corner Bézier patch S_i on side Γ_i.

We now derive the second-order derivatives of the BB patch with respect to u_i and v_i on side Γ_i, using Equations (9), (10) and (13).

$$\begin{aligned}
\left.\frac{\partial^2 S^{d,n,3}}{\partial u_i^2}\right|_{\Gamma_i} &= \left.\frac{\partial^2 S_i}{\partial u_i^2}\right|_{\Gamma_i},\\
\left.\frac{\partial^2 S^{d,n,3}}{\partial u_i \partial v_i}\right|_{\Gamma_i} &= \left.\frac{\partial^2 S_i}{\partial u_i \partial v_i}\right|_{\Gamma_i} - \left.(\alpha_{i+1}\frac{\partial^2 v_{i+1}}{\partial u_i \partial v_i}\cdot\frac{\partial S_i}{\partial u_i})\right|_{\Gamma_i},\\
\left.\frac{\partial^2 S^{d,n,3}}{\partial v_i^2}\right|_{\Gamma_i} &= \left.\frac{\partial^2 S_i}{\partial v_i^2}\right|_{\Gamma_i} + \left.(\alpha_{i+1}\frac{\partial^2 u_{i+1}}{\partial v_i^2}\cdot\frac{\partial S_i}{\partial v_i})\right|_{\Gamma_i}.
\end{aligned} \tag{16}$$

According to the surface theory in differential geometry (Farin, 1993), using Equations (15) and (16), we can obtain the six coefficients of the first and second fundamental forms for each $S^{d,n,3}$ and S_i in the u_i, v_i-plane, denoted by E, F, G, L, M, N, and $E_i, F_i, G_i, L_i, M_i, N_i$.

Then, coefficients of the first fundamental forms are obtained.

$$\begin{aligned}
E\big|_{v_i=0} &= \left.(\frac{\partial S^{d,n,3}}{\partial u_i}\cdot\frac{\partial S^{d,n,3}}{\partial u_i})\right|_{\Gamma_i} = \left.(\frac{\partial S_i}{\partial u_i}\cdot\frac{\partial S_i}{\partial u_i})\right|_{\Gamma_i} = E_i\big|_{v_i=0},\\
F\big|_{v_i=0} &= \left.(\frac{\partial S^{d,n,3}}{\partial u_i}\cdot\frac{\partial S^{d,n,3}}{\partial v_i})\right|_{\Gamma_i} = \left.(\frac{\partial S_i}{\partial u_i}\cdot\frac{\partial S_i}{\partial v_i})\right|_{\Gamma_i} = F_i\big|_{v_i=0},\\
G\big|_{v_i=0} &= \left.(\frac{\partial S^{d,n,3}}{\partial v_i}\cdot\frac{\partial S^{d,n,3}}{\partial v_i})\right|_{\Gamma_i} = \left.(\frac{\partial S_i}{\partial v_i}\cdot\frac{\partial S_i}{\partial v_i})\right|_{\Gamma_i} = G_i\big|_{v_i=0}.
\end{aligned} \tag{17}$$

Let $\mathbf{n}$ be the unit normal vector along the boundary curve that is perpendicular to the tangent plane spanned by $\frac{\partial S^{d,n,3}}{\partial u_i}\big|_{\Gamma_i}$ and $\frac{\partial S^{d,n,3}}{\partial v_i}\big|_{\Gamma_i}$, which can be expressed as

$$\mathbf{n} = \frac{\frac{\partial S^{d,n,3}}{\partial u_i}\big|_{\Gamma_i} \times \frac{\partial S^{d,n,3}}{\partial v_i}\big|_{\Gamma_i}}{\big|\big|\frac{\partial S^{d,n,3}}{\partial u_i}\big|_{\Gamma_i} \times \frac{\partial S^{d,n,3}}{\partial v_i}\big|_{\Gamma_i}\big|\big|} = \frac{\frac{\partial S_i}{\partial u_i}\big|_{\Gamma_i} \times \frac{\partial S_i}{\partial v_i}\big|_{\Gamma_i}}{\big|\big|\frac{\partial S_i}{\partial u_i}\big|_{\Gamma_i} \times \frac{\partial S_i}{\partial v_i}\big|_{\Gamma_i}\big|\big|}.$$

Then, we can obtain values of the coefficients of the second fundamental forms using Equation (16). By dot-multiplying both sides of Equation (16) with $\mathbf{n}$, the second terms on the right-hand sides of the second and third equations in (16) are eliminated.

$$\begin{aligned}
L\big|_{v_i=0} &= \left.\frac{\partial^2 S^{d,n,3}}{\partial u_i^2}\right|_{\Gamma_i}\cdot\mathbf{n} = \left.\frac{\partial^2 S_i}{\partial u_i^2}\right|_{\Gamma_i}\cdot\mathbf{n} = L_i\big|_{v_i=0},\\
M\big|_{v_i=0} &= \left.\frac{\partial^2 S^{d,n,3}}{\partial u_i \partial v_i}\right|_{\Gamma_i}\cdot\mathbf{n} = \left.\frac{\partial^2 S_i}{\partial u_i \partial v_i}\right|_{\Gamma_i}\cdot\mathbf{n} = M_i\big|_{v_i=0},\\
N\big|_{v_i=0} &= \left.\frac{\partial^2 S^{d,n,3}}{\partial v_i^2}\right|_{\Gamma_i}\cdot\mathbf{n} = \left.\frac{\partial^2 S_i}{\partial v_i^2}\right|_{\Gamma_i}\cdot\mathbf{n} = N_i\big|_{v_i=0}.
\end{aligned} \tag{18}$$

It is clear that on side Γ_i, the BB patch $S^{d,n,3}$ and the corner Bézier patch S_i have the same first and second fundamental forms in the u_i, v_i-plane. Thus, it can be inferred that $S^{d,n,3}$ has the same curvature as that of S_i along the boundary.

In conclusion, the BB patch behaves like an ordinary Bézier patch on each boundary. Thus, BB patches can be easily included in surface patchwork involving the use of Bézier surfaces.

4. Examples

In this section, we present some test examples, including the challenging configurations — the quad-net obstacle course (Peters, 2017) — to show the features of the BB patches. We also make comparisons with Gregory patch (Gregory and Hahn, 1989), extended G^2 Gregory patch (Salvi and Várady, 2014), and the GB patch (Várady et al., 2017).

4.1. Obstacle course of Peters

Fig. 7 shows the challenging model **house5**, which has a five-sided patch surrounded by ordinary Bézier patches. Different resulting multi-sided patches generated by the different methods mentioned above are demonstrated. The mean curvature and reflection line renderings are also provided to demonstrate the different visual characteristics of these methods. Similarly, Figs. 8, 9, and 10 show the **smbeam6** (6-sided), **monk7** (7-sided), and **kpa8** (8-sided) models, respectively.

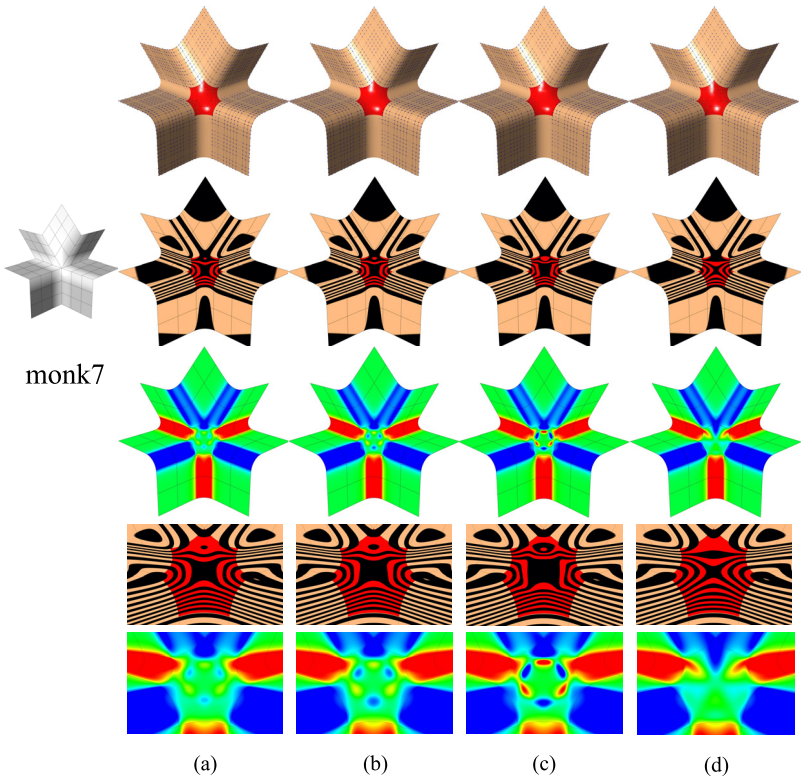

Fig. 9. monk7. Fill a 7-sided hole with G^2 continuity in different methods. (a) The BB patch; (b) Gregory patch (Gregory and Hahn, 1989); (c) extended G^2 Gregory patch (Salvi and Várady, 2014); (d) the GB patch (Várady et al., 2017). From top to bottom: shaded multi-sided patch with surrounding regular patches, reflection lines, mean curvature, close-up of reflection lines and close-up of mean curvature.

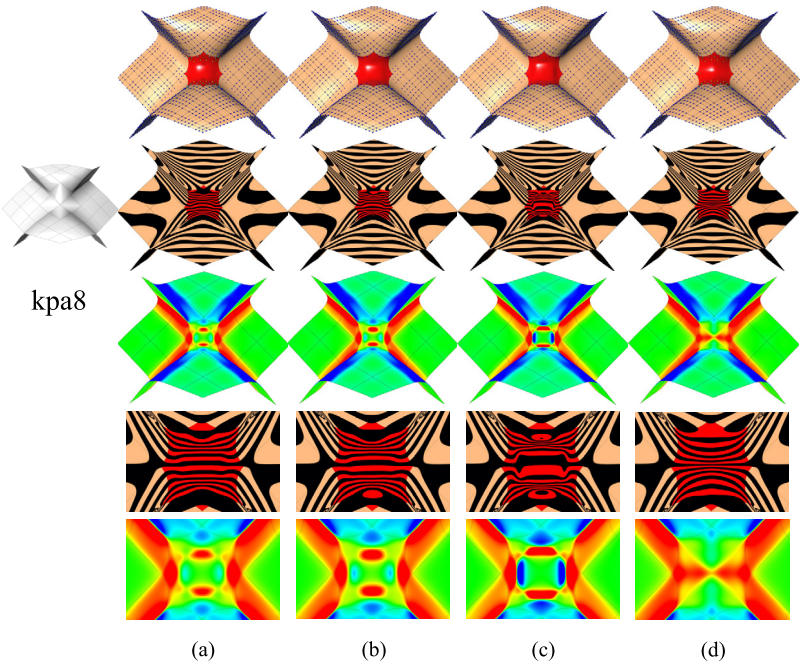

Fig. 10. kpa8. Fill an 8-sided hole with G^2 continuity in different methods. (a) The BB patch; (b) Gregory patch (Gregory and Hahn, 1989); (c) extended G^2 Gregory patch (Salvi and Várady, 2014); (d) the GB patch (Várady et al., 2017). From top to bottom: shaded multi-sided patch with surrounding regular patches, reflection lines, mean curvature, close-up of reflection lines and close-up of mean curvature.

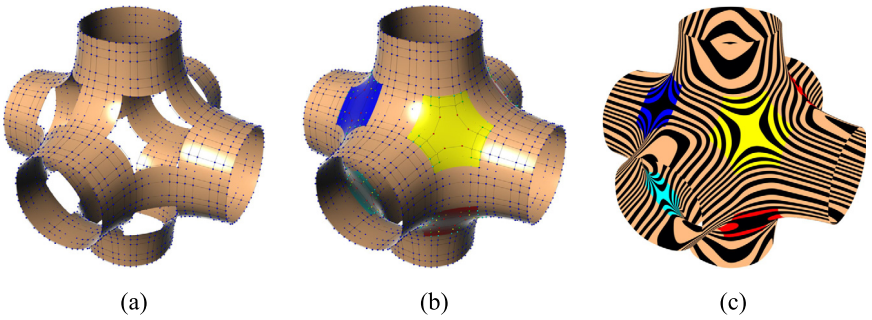

Fig. 11. "Six-way pipe" model with G^2 continuity. (a) the model with holes; (b) the hole-filled model with control points; (c) reflection lines.

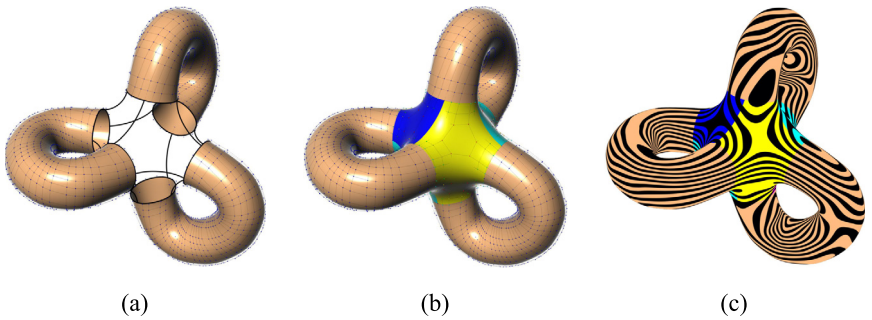

Fig. 12. "X-8" model with G^2 continuity. (a) three "U"-tubes; (b) solved model with control points; (c) reflection lines.

From the mean curvature and reflection line renderings, we can find that the BB patches have a better curvature distribution in the interior and its reflection lines have less fluctuations than Gregory and G^2 Gregory patches, which use traditional Boolean-sum Taylor interpolants. However, it appears that the GB patches behave best in the interior because its reflection lines pass through the inside in a fairly smooth manner (without any fluctuation).

4.2. Multi-sided surface modeling with BB patches

Here, we present some multi-sided surface modeling examples solved using BB patches.

A "six-way pipe" surface model with eight six-sided holes is shown in Fig. 11 (a), where each hole is surrounded by six quadrilateral Bézier patches. We used six-sided BB patches to fill these holes with G^2 continuity (see Figs. 9 (b)-(c)).

Another example is the "X-8" model, whose three "U"-tubes are separated, as shown in Fig. 12 (a). We used eight six-sided BB patches to create natural transitions between the three "U"-tubes. Each six-sided BB patch is surrounded by three quadrilateral Bézier patches and three six-sided BB patches (Fig. 12 (b)). Note that G^2 smoothness was also guaranteed in this case (Fig. 12 (c)).

In Fig. 13, four complex free-form surface models generated from the input closed quadmeshes with arbitrary topology are shown. We constructed the Bézier control nets (including multi-sided Bézier nets) from the input quadmeshes. The reflection lines indicate that the union of all of these surface patches is G^2 continuous.

5. Discussion

In this section, we discuss the limitations of the BB patch and future work.

1. As mentioned above, we assume that the twist compatibility of the multi-sided Bézier control net and the corresponding control points at each corner must be the same. However, if the input grid encounters twist incompatibility at the corner, then the inner control points at the corner are not identical. Hall and Mullineux (1999b) first used this type of multi-sided Bézier control net, which was derived from Chiyokura and Kimura's method Chiyokura and Kimura (1983), to generalize the control point construction of Zheng and Ball (1997) to allow incompatible twist vectors. Recently, Hettinga and Kosinka (2018) used Chiyokura and Kimura's method (Chiyokura and Kimura, 1983) to generate Gregory GB and S-patches that can address the twist incompatibility problem. For the BB scheme, we likewise may be able to define a special Bézier patch by using Chiyokura and Kimura's method (Chiyokura and Kimura, 1983) instead of an ordinary Bézier patch at each corner; thus, the final BB patch would be able to handle twist incompatibility.
2. A BB patch is defined over a regular polygonal domain; however, mapping a 2D regular polygon to an irregular 3D region may result in unexpected shape artifacts. A previous research (Várady et al., 2011) has investigated this problem

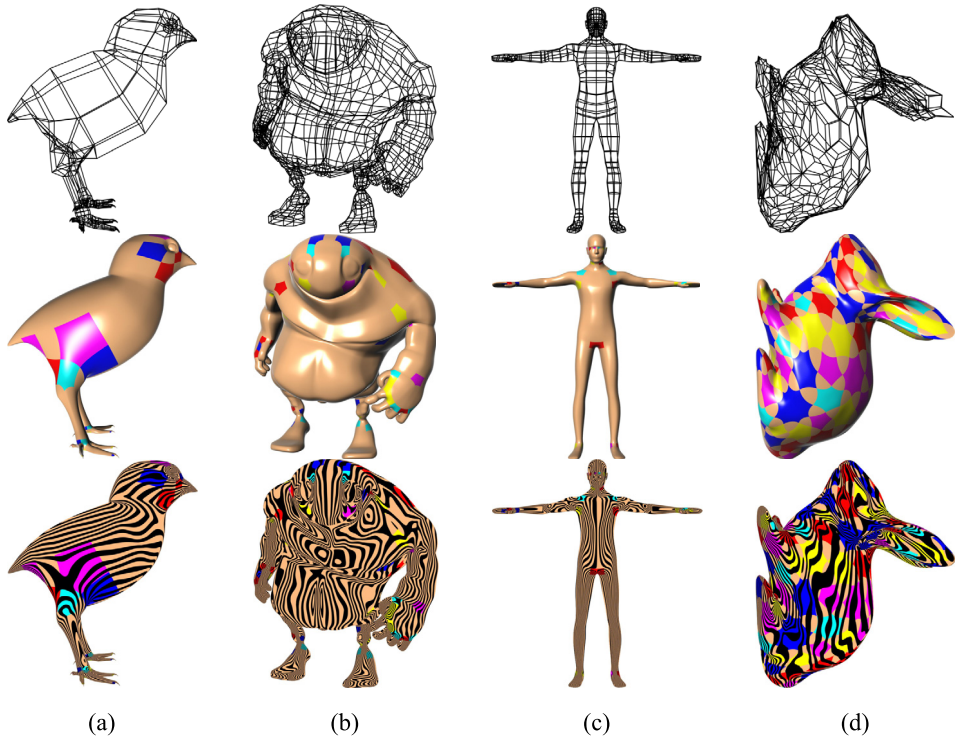

Fig. 13. Free-form surface models with G^2 continuity. From top to bottom: input quadrilateral meshes, shaded surface models and reflection lines.

and recommended the use of irregular polygonal domains based on the boundary configuration to improve surface quality. Furthermore, Salvi and Várady (2018) created their multi-sided surfaces over non-convex polygonal domains when the boundary segments had 3D concave angles. However, owing to the corner blending scheme, it seems difficult to define BB patches over concave domains.

3. In this study, we did not include the case of a three-sided patch. This is because each defined corner grid is a four-sided grid, which reduces the n-sided grid. A three-sided grid does not have sufficient control points to be reduced to a four-sided grid. In contrast, constrained sweep parameterization is unsuitable for the triangular domain because the solution of the Equation (3) is not unique in this case. To construct a fairly good three-sided BB patch, an appropriate rule for constructing the corner grids from a three-sided control net and a well-defined parameterization over the triangular domain must be determined.
4. In addition, owing to the simple control structure of the BB scheme, it would be easy to generate multi-sided patches with B-spline boundaries. We should mention there have been some multi-sided control point-based B-spline patches, which based on the GB scheme (Hettinga and Kosinka, 2020a,b; Vaitkus et al., 2021).

6. Conclusion

We introduced the BB patch, a new multi-sided Bézier patch with a simple and intuitive control structure based on Gregory corner interpolant. A BB patch can be easily connected to a quadrilateral Bézier patch or another BB patch with G^2 continuity. When the number of sides was reduced to four, the BB patch became an ordinary quadrilateral Bézier patch.

In the near future, we plan to extend the BB patches from regular polygonal domains to general domains, construct appropriate three-sided patches, and extend the scheme to create multi-sided B-spline surface patches.

CRediT authorship contribution statement

Kaikai Qin: Methodology, Software, Visualization, Writing – original draft, Writing – review & editing. **Yajuan Li:** Methodology, Supervision, Writing – original draft, Writing – review & editing. **Chongyang Deng:** Conceptualization, Funding acquisition, Methodology, Software, Supervision, Visualization, Writing – original draft, Writing – review & editing.

Declaration of competing interest

The authors declare that they have no known competing financial interests or personal relationships that could have appeared to influence the work reported in this paper.

Data availability

No data was used for the research described in the article.

Acknowledgements

The authors wish to thank all anonymous referees for their valuable comments and suggestions. This work was supported by the National Natural Science Foundation of China (NSFC) under the project numbers 61872121.

References

Goldman, Ron, 2004. Multisided arrays of control points for multisided Bézier patches. Comput. Aided Geom. Des. 21 (3), 243–261.
Peters, Jörg, 2019. Splines for meshes with irregularities. SMAI J. Comput. Math.
Salvi, Péter, Tamás, Várady, Alyn, Rockwood, 2014. Ribbon-based transfinite surfaces. Comput. Aided Geom. Des. 31 (9), 613–630.
Várady, Tamás, Salvi, Péter, Karikó, György, 2016. A multi-sided Bézier patch with a simple control structure. Comput. Graph. Forum 35 (2), 307–317.
Várady, Tamás, Salvi, Péter, Kovács, István, 2017. Enhancement of a multi-sided Bézier surface representation. Comput. Aided Geom. Des. 55, 69–83.
Salvi, Péter, Várady, Tamás, 2018. Multi-sided Bézier surfaces over concave polygonal domains. Comput. Graph. 74, 56–65.
Charrot, Peter, Gregory, John A., 1984. A pentagonal surface patch for computer aided geometric design. Comput. Aided Geom. Des. 1 (1), 87–94.
Gregory, John A., Hahn, Jörg M., 1989. A C2 polygonal surface patch. Comput. Aided Geom. Des. 6 (1), 69–75.
Catmull, Edwin, Clark, James, 1978. Recursively generated B-spline surfaces on arbitrary topological meshes. Comput. Aided Des. 10 (6), 350–355.
Karčiauskas, Kestutis, Peters, Jörg, 2007. Concentric tessellation maps and curvature continuous guided surfaces. Comput. Aided Geom. Des. 24 (2), 99–111.
Gregory, John A., Zhou, Jianwei, 1994. Filling polygonal holes with bicubic patches. Comput. Aided Geom. Des. 11 (4), 391–410.
Peters, Jörg, 1999. Constructing C1 surfaces of arbitrary topology using biquadratic and bicubic splines.
Loop, Charles, Schaefer, Scott, 2008. G2 tensor product splines over extraordinary vertices. Comput. Graph. Forum 27 (5), 1373–1382.
Karčiauskas, Kestutis, Peters, Jŕg, 2016. Minimal bi-6 G2 completion of bicubic spline surfaces. Comput. Aided Geom. Des. 41, 10–22.
Karčiauskas, Kestutis, Peters, Jörg, 2020. A sharp degree bound on G2-refinable multi-sided surfaces. Comput. Aided Des. 125, 102867.
Kato, Kiyokata, 1991. Generation of N-sided surface patches with holes. Comput. Aided Des. 23 (10), 676–683.
Várady, Tamas, 1991. Overlap patches: a new scheme for interpolating curve networks with n-sided regions. Comput. Aided Geom. Des. 8 (1), 7–27.
Várady, Tamás, Rockwood, Alyn, Salvi, Péter, 2011. Transfinite surface interpolation over irregular n-sided domains. In: Solid and Physical Modeling. Comput. Aided Des. 43 (11), 1330–1340.
Salvi, Péter, Várady, Tamás, 2014. G2 surface interpolation over general topology curve networks. Comput. Graph. Forum 33 (7), 151–160.
Sabin, Malcolm A., 1983. Non-rectangular surface patches suitable for inclusion in a B-spline surface. In: ten Hagen, P.J.W. (Ed.), Eurographics Conference Proceedings. The Eurographics Association.
Hosaka, Mamoru, Kimura, Fumihiko, 1984. Non-four-sided patch expressions with control points. Comput. Aided Geom. Des. 1 (1), 75–86.
Zheng, Jinjin, Ball, Alan A., 1997. Control point surfaces over non-four-sided areas. Comput. Aided Geom. Des. 14 (9), 807–821.
Loop, Charles T., DeRose, Tony D., 1989. A multisided generalization of Bézier surfaces. ACM Trans. Graph. 8 (3), 204–234.
Warren, Joe, 1992. Creating multisided rational Bézier surfaces using base points. ACM Trans. Graph. 11 (2), 127–139.
Hall, Richard, Mullineux, Glen, 1999a. Continuity between Gregory-like patches. Comput. Aided Geom. Des. 16 (3), 197–216.
Farin, Gerald, 1993. Chapter 22 - W. Boehm: differential geometry II. In: Farin, Gerald (Ed.), Curves and Surfaces for Computer-Aided Geometric Design (Third Edition), third edition. Academic Press, Boston, pp. 389–405.
Peters, Jörg, 2017. Quad-Net Obstacle Course. Website. https://www.cise.ufl.edu/research/SurfLab/shape_gallery.shtml.
Hall, Richard, Mullineux, Glen, 1999b. The Zheng–ball construction without twist constraints. Comput. Aided Geom. Des. 16 (3), 165–175.
Chiyokura, Hiroaki, Kimura, Fumihiko, 1983. Design of solids with free-form surfaces. SIGGRAPH Comput. Graph. 17 (3), 289–298.
Hettinga, Gerben J., Kosinka, Jiří, 2018. Multisided generalisations of Gregory patches. Comput. Aided Geom. Des. 62, 166–180.
Hettinga, Gerben J., Kosinka, Jiří, 2020a. A multisided C2 b-spline patch over extraordinary vertices in quadrilateral meshes. Comput. Aided Des. 127, 102855.
Hettinga, Gerben J., Kosinka, Jiri, 2020b. Multisided B-spline patches over extraordinary regions. In: Biasotti, Silvia, Pintus, Ruggero, Berretti, Stefano (Eds.), Smart Tools and Apps for Graphics - Eurographics Italian Chapter Conference. The Eurographics Association.
Vaitkus, Márton, Várady, Tamás, Salvi, Péter, Sipos, Ágoston, 2021. Multi-sided B-spline surfaces over curved, multi-connected domains. Comput. Aided Geom. Des. 89, 102019.